5670–5683 *Nucleic Acids Research, 2019, Vol. 47, No. 11* *Published online 5 April 2019*
doi: 10.1093/nar/gkz226

SCRE serves as a unique synaptonemal complex fastener and is essential for progression of meiosis prophase I in mice

Hongbin Liu[1,2,†], Tao Huang[1,†], Mengjing Li[1,†], Miao Li[1], Chuanxin Zhang[1], Jing Jiang[3], Xiaochen Yu[1], Yingying Yin[1], Fan Zhang[3], Gang Lu[2], Meng-Cheng Luo[4], Liang-Ran Zhang[1], Jinsong Li[3], Kui Liu[1,5] and Zi-Jiang Chen[1,6,*]

[1]Center for Reproductive Medicine, Shandong University, Jinan, China; The Key Laboratory of Reproductive Endocrinology of Ministry of Education, Jinan, China; National Research Center for Assisted Reproductive Technology and Reproductive Genetics, Jinan, China, [2]CUHK-SDU Joint Laboratory on Reproductive Genetics, School of Biomedical Sciences, the Chinese University of Hong Kong, Hong Kong, China, [3]Genome Tagging Project (GTP) Center, State Key Laboratory of Cell Biology, Shanghai Key Laboratory of Molecular Andrology, CAS Center for Excellence in Molecular Cell Science, Shanghai Institute of Biochemistry and Cell Biology, Chinese Academy of Sciences, University of Chinese Academy of Sciences, Shanghai, China, [4]Department of Tissue and Embryology, School of Basic Medical Sciences, Wuhan University, Wuhan, China, Hubei Provincial Key Laboratory of Developmentally Originated Disease, Wuhan, China, [5]Department of Obstetrics and Gynecology, Li Ka Shing Faculty of Medicine, The University of Hong Kong, Hong Kong, China; Shenzhen Key Laboratory of Fertility Regulation, Center of Assisted Reproduction and Embryology, The University of Hong Kong - Shenzhen Hospital, Haiyuan First Road 1, Shenzhen 518053, China and [6]Shanghai Key Laboratory for Assisted Reproduction and Reproductive Genetics, Shanghai, China

Received January 20, 2019; Revised March 19, 2019; Editorial Decision March 20, 2019; Accepted March 22, 2019

ABSTRACT

Meiosis is a specialized cell division for producing haploid gametes from diploid germ cells. During meiosis, synaptonemal complex (SC) mediates the alignment of homologs and plays essential roles in homologous recombination and therefore in promoting accurate chromosome segregation. In this study, we have identified a novel protein SCRE (synaptonemal complex reinforcing element) as a key molecule in maintaining the integrity of SC during meiosis prophase I in mice. Deletion of *Scre* (*synaptonemal complex reinforcing element*) caused germ cell death in both male and female mice, resulting in infertility. Our mechanistic studies showed that the synapses and SCs in *Scre* knockout mice were unstable due to the lack of the SC reinforcing function of SCRE, which is sparsely localized as discrete foci along the central elements in normal synaptic homologous chromosomes. The lack of *Scre* leads to meiosis collapse at the late zygotene stage. We further showed that SCRE interacts with synaptonemal complex protein 1 (SYCP1) and synaptonemal complex central element 3 (SYCE3). We conclude that the function of SCRE is to reinforce the integrity of the central elements, thereby stabilizing the SC and ensuring meiotic cell cycle progression. Our study identified SCRE as a novel SC fastener protein that is distinct from other known SC proteins.

INTRODUCTION

Meiosis is a specialized cell division for producing haploid gametes from diploid germ cells. The progression of meiosis is unique among extant eukaryotes and is crucial for increasing genetic diversity. Despite the massive amount of variation seen in different organisms, meiosis-specific steps are generally conserved. During meiosis, two successive rounds of chromosome segregation occur following a single round of replication, resulting in the formation of haploid gametes from diploid progenitors, and to ensure their accurate segregation, homologous chromosomes must pair and undergo crossover recombination (1–3).

Meiotic recombination involves several steps, including formation of double-strand breaks (DSBs), exonucleolytic resection of 5′ ends at the breaks, and strand invasion into a chromatid of the homologous chromosome (1,4,5). In all

*To whom correspondence should be addressed. Tel: +86 0531 85651190; Fax: +86 0531 87068226; Email: Chenzijiang@hotmail.com
†The authors wish it to be known that, in their opinion, the first three authors should be regarded as joint First Authors.

organisms studied so far, the formation of meiotic DSBs is catalyzed by the topoisomerase-like protein SPO11 (6–8), and the resulting single-stranded DNA is protected from degradation by the replication protein A complex (RPA1, 2 and 3) (9,10). With the assistance of the RAD51 and DMC1 recombinases, annealed DSB ends develop into an extended D-loop (11), and the DSBs are then repaired by either the crossover or non-crossover pathway (12,13).

Crossovers are the final outcome of a meiotic DSB repair mechanism, in which the stabilization of SC is indispensable (7,14). The formation of the multi-protein SC structure is initiated during leptonema when synaptonemal complex proteins 2 and 3 (SYCP2 and SYCP3) begin to form the axial elements (AEs). Subsequently, when the homologous chromosomes become synapsed at the zygotene stage, the lateral elements (LEs) are joined by transverse filaments formed by SYCP1 and five other known central elements (CEs), including synaptonemal complex central element 1(SYCE1), SYCE2, SYCE3, testis expressed 12 (TEX12), and SIX6OS1 (For reviews, see (15–17). Spermatocytes from *Sycp2* or *Sycp3* knockout mice exhibit severe abnormalities in axial formation (15), and spermatocytes from mice lacking *Sycp1*, *Syce1*, *Syce2*, *Syce3*, *Tex12* and *Six6os1* suffer complete failure of synapsis and therefor the absence of completed crossovers (16–20). Among the components listed above, SYCP1, SYCE1, SYCE3 and SIX6OS1 are believed to be responsible for initiating the assembly of the SC, whereas SYCE2 and TEX12 constitute a hetero-octamer complex that is essential for synapsis extension (16,19–21). Thus, all the above-mentioned proteins are essential for the proper formation of SCs.

In this study, we have identified a novel protein SCRE (synaptonemal complex reinforcing element) as a key component in maintaining the integrity of SC during meiosis prophase I in germ cells of mice. However, unlike all other known SC components with a continuous expression pattern, SCRE appears as a sparsely distributed pattern of discrete foci along the synapsed axes of homologous chromosomes only from the zygotene to early diplotene stages of meiosis prophase I. Our results showed that upon depletion of *Scre* in mice, the SC can form but rapidly collapses with a complete lack of meiotic crossover formation, resulting in infertility in mice. Therefore, SCRE is not needed for the initiation of SC formation but is indispensable for the stabilization of the SC. This role of SCRE is distinct from all known SC proteins, including SYCP1, SYCE1, SYCE2, SYCE3, SIX6OS1 and TEX12 (16,20,22).

MATERIALS AND METHODS

Production of CRISPR/Cas9-edited *Scre* gene knockout mice

The mouse *Scre* gene (Transcript: ENSMUSG00000089798), composed of 13.67 kb, is located on chromosome 5. Six exons have been identified, with an ATG start codon in exon 2 and a TGA stop codon in exon 6. The knockout mouse was created using a CRISPR/Cas9-mediated genome editing system from Cyagen Biosciences. Exon 3 and exon 6 were selected as the target sites. By co-injecting gRNA and *Cas9* mRNA into fertilized eggs of C57BL/6 mice, we generated two mutant lines—one with a 5005 base deletion and one point mutation (A>T), and one with a 4982 base deletion and 11 point mutations (TCCTTCCGTTTCAGT>CTCCTCTGAAGTGAA). The founders were genotyped by PCR followed by DNA sequencing analysis. Intercrossing of *Scre* heterozygous mice yielded healthy offspring at Mendelian ratios. The use of mice was approved by the Animal Ethics Committee of the School of Medicine, Shandong University. All animal care protocols and experiments were reviewed and approved by the Animal Use Committee of the School of Medicine, Shandong University.

Genotyping

Genotyping was performed by PCR amplification of genomic DNA extracted from mouse tails. The PCR primers for the *Scre* mutant allele were Forward: 5′-GAT TTC CAG ACC ACA CTC AGA ACT TCA G-3′ and Reverse: 5′-CAG GTC TTA CAT TCC GCT CTC TTC AC-3′, yielding a 464 bp fragment. PCR primers for *Scre* wild-type allele were Forward: 5′-GAT TTC CAG ACC ACA CTC AGA ACT TCA G-3′ and Reverse: 5′-AAT ACC GAA CCT TGT GGC TTC GAT-3′, yielding a 266 bp fragment.

Production of CRISPR/Cas9- edited HA-tag *Scre* knockin mice

Plasmid construction. To generate the CRISPR-Cas9 plasmid for HA-tag knockin (KI), sgRNAs of the N-terminus of the target gene *Scre* (CTC ATC CAT TGC CAT GCC GC) were synthesized, annealed and ligated to the pX330-*mCherry* plasmid (Addgene, #98750), which had been digested with Bbs I (Thermo). For the construction of the HA-tag KI DNA donor, the sequences encoding the left homologous arm, the HA tag, and the right homologous arm were amplified and ligated to the linear pMD19T vector with a 20 bp overlap using the Seamless Cloning Kit (Beyotime, D7010S).

Cell culture and transfection. DKO-AG-haESCs were maintained in DMEM (Millipore) with 15% FBS (Gibco), penicillin/streptomycin, non-essential amino acids, L-glutamine, nucleosides, 2-mercaptoethanol, 1000 U/ml Lif, 1 μM PD03259010 (Selleck) and 3 μM CHIR99021 (Selleck). Cells were passaged every 2–3 days (23). DKO-AG-haESCs were transfected with CRISPR-Cas9 plasmid and HA tag KI DNA donor using Lipofectamine 2000 (Life Technologies). At 24 h after transfection, the mCherry-positive haploid cells were enriched by fluorescence-activated cell sorting (FACS, BD AriaII) and plated at a low density. In 7–8 days after plating, single colonies were picked up, and positive colonies for the HA tag were selected by genomic DNA PCR amplification for Sanger sequencing.

ICAHCI and Scre-*N-HA semi-cloned mouse generation.* To generate semi-cloned embryos, DKO-AG-haESCs with *Scre*-N-HA were arrested in M-phase by culturing in medium containing 0.05 μg/ml demecolcine for 10 h and then used for intracytoplasmic injection as described previously (23). ICAHCI embryos were cultured in KSOM

medium for 24 h to reach the two-cell stage. A total of 15–20 two-cell embryos were transferred into each oviduct of pseudo-pregnant ICR females at 0.5 days post-coitus (dpc). *Scre*-N-HA semi-cloned mice (F0) were crossed with WT C57BL/6J male mice to generate heterozygous *Scre*-N-HA F1 male mice for our experiments.

Purification of male germ cells

The purification of male germ cells was performed as described previously (24). The cell type and purity in each fraction were assessed based on their diameters and morphological characteristics under a light microscope.

Tissue collection and histological analysis

Testes from at least three mice for each genotype were dissected immediately after euthanasia, fixed in 4% (mass/vol) paraformaldehyde (Solarbio, Beijing, China, P1110) for up to 24 h, stored in 70% (vol/vol) ethanol, and embedded in paraffin. Five μm sections were prepared and mounted on glass slides. After deparaffinization, slides were stained with hematoxylin for histological analysis. For TUNEL staining, we followed the manufacturer's instructions (keyGEN BioTECH, #KGA7072).

Exogenous expression of *Scre* cDNAs in testes

Full length *Scre* cDNA were cloned into the pCAG-GFP vector (Addgene #11150). Plasmid DNA was injected into live mouse testes, and the exogenous expression was achieved by electroporation as previously described (25). Spermatocytes expressing the exogenous genes were detected by immunostaining of GFP.

Immunostaining and antibodies

Spermatocyte spreads were prepared as previously described (26). Oocytes from fetal ovaries (E17.5 embryos) were digested with collagenase, incubated in hypotonic buffer, disaggregated, fixed in paraformaldehyde, and incubated with the indicated antibodies for immunofluorescent staining. Primary antibodies used for immunostaining were as follows: rabbit anti-SCP3 (1:500 dilution; Abcam #ab15093), mouse anti-SCP3 (1:500 dilution; Abcam #ab97672), rabbit anti-SCP1 (1:2000 dilution; Abcam # ab15090), rabbit anti-SCP1 (1:2000 dilution; Abclonal #A12139), rabbit anti-SYCE3 (this antibody was raised against the conserved polypeptide CKEEMEKNWQELLTETKRKQ), rabbit anti-RPA2 (1:200 dilution; Abcam #ab76420), rabbit anti-RAD51 (1:200 dilution; Thermo Fisher Scientific #PA5-27195), rabbit anti-DMC1 (1:100 dilution; Santa Cruz Biotechnology #sc-22768), mouse anti-phospho-Histone H2A.X (Ser139), clone JBW301 (1:300 dilution; Millipore #05-636), mouse anti-MLH1 (1:50 dilution; BD Biosciences #550838), rabbit anti-GFP (1:500 dilution; Thermo Fisher Scientific #A11122), and rabbit anti-HA (1:100 dilution, Cell Signaling Technology #372). Primary antibodies were detected with Alexa Fluor 488-, 594-, or 647-conjugated secondary antibodies (1:500 dilution, Thermo Fisher Scientific #A-11070, Abcam #ab150084, #ab150067, #ab150113, #ab150120, #ab150119, #ab150165, #ab150168 and #ab150167) for 1 h at room temperature. The slides were washed several times with PBS and mounted using VECTASHIELD medium with DAPI (Vector Laboratories, # H-1200).

Generation of plasmids

Full-length cDNAs encoding SYCP1, SYCE3, SYCE1, TEX12, SYCE2 and SYCP3 were amplified by RT-PCR from murine testis RNA. Full-length cDNAs were cloned into the pcDNA3.1, PCAG and PCMW6 mammalian expression vectors.

Immunoprecipitation and antibodies

HEK 293T cells were transiently transfected using X-tremeGENE HP DNA Transfection Reagent (Roche). Transfected cells were lysed in TAP lysis buffer (50 mM HEPES–KOH, pH 7.5, 100 mM KCl, 2 mM EDTA, 10% glycerol, 0.1% NP-40, 10 mM NaF, 0.25 mM Na_3VO_4, 50 mM β-glycerolphosphate) plus protease inhibitors (Roche, 04693132001) for 30 min on ice and then centrifuged at 13 000 × *g* for 15 min. The antibody was added and the mixture was rotated in Eppendorf tubes at 4°C overnight, and immunocomplexes were isolated by adsorption to protein A/G Sepharose beads for 1 h. After washing, the beads were loaded onto 4–20% Tris-Glycine Mini Gels (Invitrogen) and separated proteins were detected by western blotting with the indicated antibodies. Immunoprecipitations were performed using rabbit anti-GFP antibody (50430-2-AP, Proteintech) and mouse anti-IgG antibody (10283-1-AP, Proteintech). Primary antibodies used for western blotting were guinea-pig SCRE antibody (this antibody was raised against the full-length protein), mouse anti-FLAG antibody (Sigma-Aldrich #F1804, 1:1000 dilution), mouse anti-GFP antibody (Proteintech #66002-1-Ig, 1:3000 dilution), mouse anti-Myc antibody (Cell Signaling Technology #2276, 1:1000 dilution), mouse anti-His antibody (Proteintech #66005-1-Ig, 1:3000 dilution), rabbit anti-β-Actin antibody (Cell Signaling Technology #4970, 1:1000 dilution). Secondary horseradish peroxidase-conjugated anti-mouse (Zhong Shan Jin Qiao) and anti-rabbit (Zhong Shan Jin Qiao) antibodies were used at 1:5000 dilution. Antibodies were detected with the Immobilon Western Chemiluminescent HRP Substrate from Millipore.

Real-time PCR

Total RNA was isolated from various tissues of wild-type or knockout adult mice. To analyze the expression of *Scre* mRNAs in various tissues and to verify the knockout efficiency, cDNA were synthesized using the PrimeScript RT reagent Kit with gDNA Eraser (Takara). qPCR was performed using TB Green Premix Ex Taq (Takara) and specific forward and reverse primers: *Scre* primer pair 1 F 5′-GGA GTG TAT GAC ATC GGC TGA-3′ and R 5′-CTG CCC AAG AAC CTC TGA TGT-3′; *Scre* primer pair 2 F 5′-TGG GCC TGA AGA ATG GAG TC-3′ and R 5′-GCT CTG CTC TAT GAT GTA CGC T-3′. β-Actin was amplified as a housekeeping gene with the primers β-actin F

5′-CAT CCG TAA AGA CCT CTA TGC CAA C-3′ and qβ-actin R 5′-ATG GAG CCA CCG ATC CAC A-3′. All RT-PCR reactions were performed with an initial denaturation at 95°C for 10 min followed by 25 cycles of denaturation at 95°C for 30 s, annealing at 60°C for 30 s, and extension at 72°C for 30 s and a final extension at 72°C for 5 min using a T100 Thermal Cycler (Bio-Rad).

Imaging

Immunostained chromosome spreads were imaged by confocal microscopy using either a Leica TCS SP5 resonant-scanning confocal microscope driven by Leica Application Suite Software, or an Andor Dragonfly spinning disc confocal microscope driven by Fusion Software. Projection images were then prepared using ImageJ Software (NIH, version 1.6.0-65) or Bitplane Imaris (version 8.1) software. Histology were analyzed with an epifluorescence microscope (BX52, Olympus), and processed using Photoshop (Adobe) software packages. super-resolution structured illumination microscopy (SIM) analysis was performed with Acquire SR software on a DeltaVision OMX SR super resolution imaging system (GE Healthcare) equipped with a 60×/1.42 oil objective, and the images were further computationally reconstructed and processed with softWoRx software (GE Healthcare) to generate super resolution optical series sections with two-fold extended resolution in both *xy* and *z* axes.

Statistical analysis

All data are presented as the mean ± SEM when possible. The statistical significance of the differences between the mean values for the different genotypes was measured by Welch's *t*-test with a paired, two-tailed distribution. The data were considered significant when the *P*-value was less than 0.05 (*) or 0.01 (**).

RESULTS

Expression of the meiosis prophase I-specific gene *Scre* in mice

Through mRNA sequencing of mouse male germ cells, we identified an unparalleled gene, coded by *1700028K03Rik*, and we named it *Scre*. We have used the **PSIPRED** database (http://bioinf.cs.ucl.ac.uk/psipred/) and sequence analysis of SCRE reveals that this 186 amino acid protein consists of 3 predicted α-helices in its C-terminal region, with a divergent N-terminus. These three predicted α-helices represent a common feature to 2 known synaptonemal complex components, SYCE2 and TEX12 (Figure 6A) (21). *Scre* was highly expressed in the adult testis, and was expressed in the embryonic ovary, both of which are organs where meiotic prophase I occurs (Figure 1A, supplementary Figure S1A). The lower level of expression in mouse embryonic ovaries is likely due to the smaller proportion of germ cells in the embryonic ovaries. To further study the functional roles of SCRE in germ cell development, we investigated the expression pattern of SCRE in different stages of male germ cells isolated by BSA gradient sedimentation (24). In the subsequent western blotting, we found that SCRE protein expression began to be observed in spermatogonia B and increased in spermatocytes at leptotene to pachytene stages and in round spermatids. Then the SCRE expression became almost undetectable in elongated spermatids (Supplementary Figure S1B).

Dynamic localization of SCRE to SCs

To further identify the functional roles of SCRE, we electroporated an expression plasmid encoding *Scre*-GFP into live mouse testes. Forty-eight hours later, we carried out a detailed analysis of mouse spermatocyte spreads through triple labeling with antibodies against GFP, SYCP3 and SYCP1. SCRE was expressed as distinct points along the chromosome axis from the zygotene to early diplotene stage, and its expression was co-localized with SYCP1 along synapsed LEs (Figure 1B–D, yellow arrows). The pseudoautosomal synapsed region (PAR) was also labeled positively for SCRE on the XY bivalent (Figure 1C, yellow arrow). As spermatocytes progressed into early diplotene stage, the SCRE (together with SYCP1) signals disappeared at the desynapsed regions (Figure 1D, red dotted circles, and inset). Then, the remaining SCRE foci were not detected during late diplotene stage (Figure 1E). Thus, our results suggest that SCRE might be closely related to chromosomal synapsis, but it has significantly different characteristics compared to other components of the SC.

We further characterized SCRE localization in spermatocytes by super-resolution structured illumination microscopy (SIM). In previous studies, antibodies that targeted either the N-terminal domain or the C-terminal domain of SYCP1 enabled each domain to be visualized independently and provided confirmation that the C-terminus of SYCP1 localizes with the lateral elements, whereas its N-terminus localizes with the central elements (27,28). By resolving the two SYCP3 staining axes of synapsed homologs, SIM imaging showed that SCRE localized specifically to the middle region of developing SCs (Figure 1F–K, arrows). To further locate the expression of SCRE along the chromosome axis, we used triple labeling with antibodies against GFP, SYCP3 and SYCP1-C (for labeling the C-terminus of SYCP1). SIM imaging showed that SCRE mainly located at the middle region of SYCP1-C (Figure 1L-S, arrows). We confirmed this result through double labeling with antibodies against GFP, SYCP1-N, SYCE3 or TEX12, which were located in the central region of SCs (27). Antibodies that targeted either SYCP1-N, SYCE3 or TEX12 provided confirmation that SCRE was distributed along the CEs and was co-localized with these molecules (Figure 1T-Y, arrows). Taken together, SCRE shows an atypical localization pattern as distinct foci along the chromosome axis, and this is different from other known SC proteins. It is possible that SCRE has some special binding properties that can localize this protein to distant foci other than the more commonly known repetitive or continuous expression pattern of SC members. We measured the distance between two adjacent foci in the same chromosomes, and the average distance was 892 nm ± 354 (s.d.; X measurements in seven cells of early pachytene) with a range of ∼400–1400

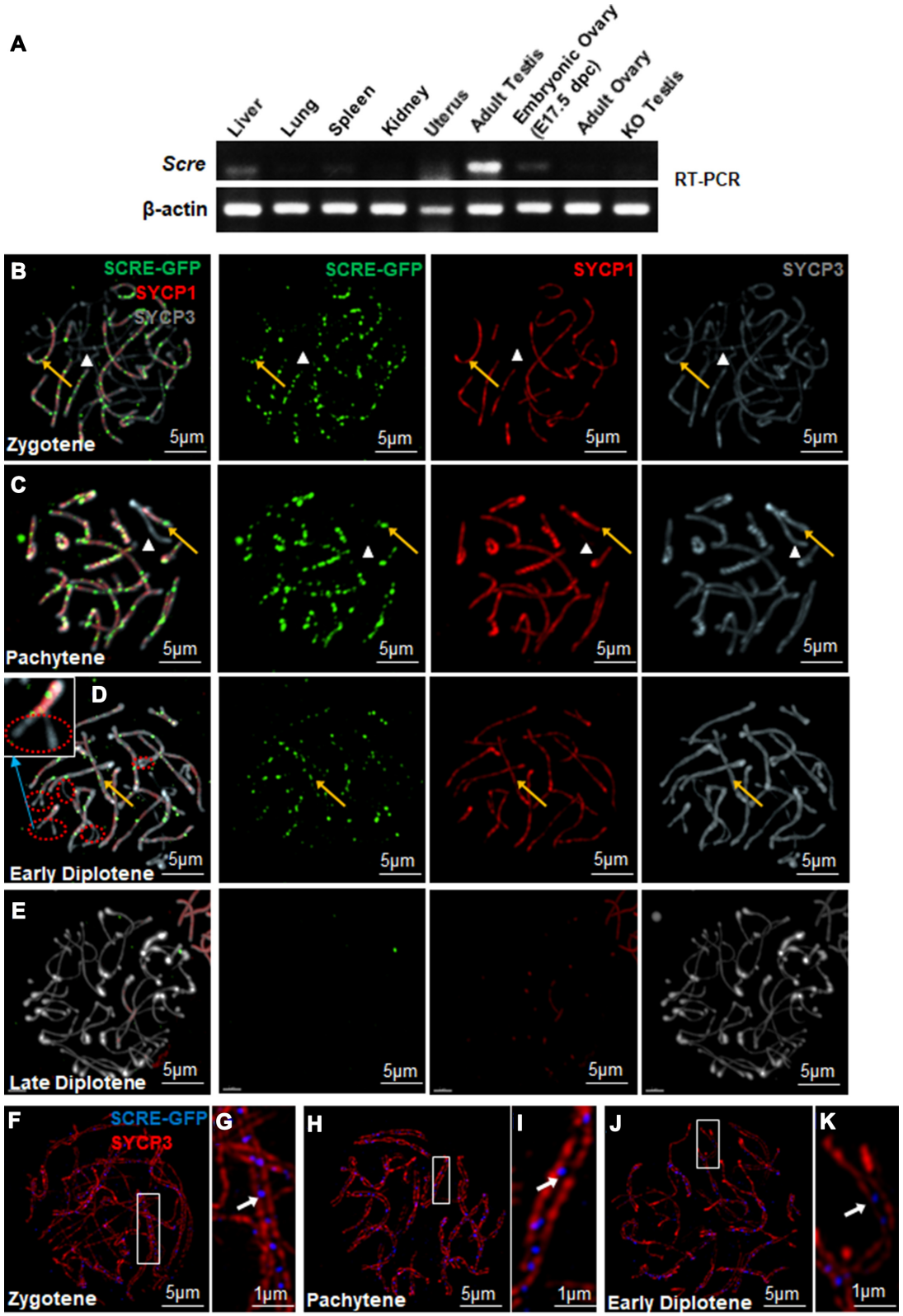
A
Liver
Lung
Spleen
Kidney
Uterus
Adult Testis
Embryonic Ovary (E17.5 dpc)
Adult Ovary
KO Testis
Scre
β-actin
RT-PCR
B
SCRE-GFP
SYCP1
SYCP3
Zygotene
5μm
C
Pachytene
D
Early Diplotene
E
Late Diplotene
F
Zygotene
G
1μm
H
Pachytene
I
J
Early Diplotene
K

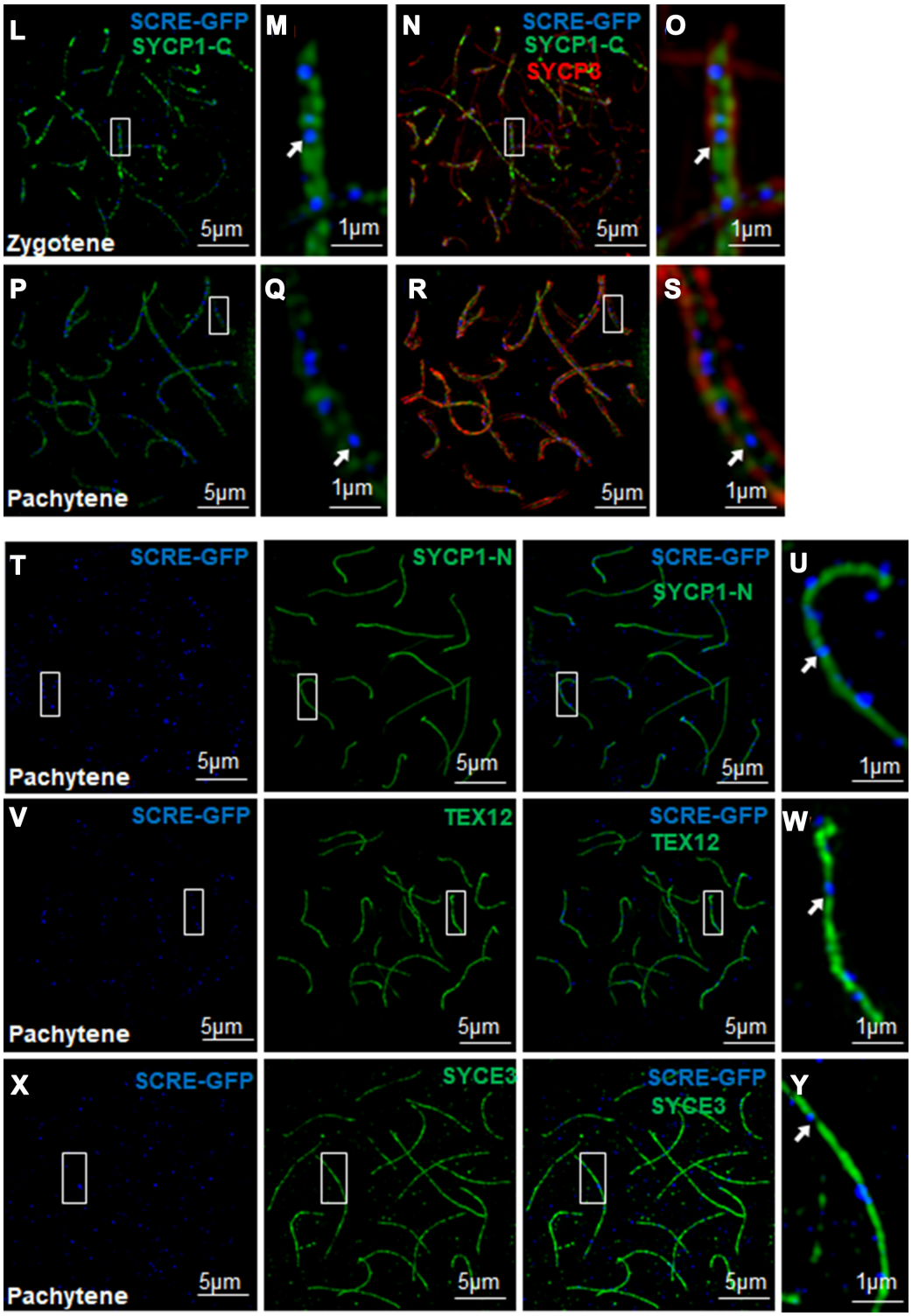

Figure 1. Transcriptional analysis and distribution of SCRE in mouse meiocytes. (**A**) RT-PCR detection of SCRE in different tissues, indicating that SCRE was highly expressed in adult testes and embryonic ovaries. (**B–E**) Dynamic localization of SCRE to SCs in mouse spermatocytes. SCRE localized to the chromosome axis as distinct foci at the (**B**) zygotene, (**C**) pachytene, (**D**) early diplotene and (**E**) late diplotene stages. SCRE expression was co-localized with SYCP1 along synapsed chromosomes (B–D, arrows) and disappeared on unsynapsed chromosomes (B–C, arrowheads; D, red dotted circles and inset). (C, arrow) The PAR of the XY bivalent was labeled for SCRE. (**F–K**) SIM images of the zygotene (**F**), pachytene (**H**), and early diplotene stage (**J**) nuclei immunolabeled for SCRE and SYCP3. (**G, I, K**) Magnified views of synapsed regions indicated by arrowheads show that SCRE was located in the intermediate region of the SC. (**L–S**) Triple immunostaining of SCRE (blue), SYCP3 (red), and SYCP1-C (green) in the zygotene (**L–O**) and pachytene (**P–S**) stages. (**O, S**) Immunofluorescence signals were acquired using SIM, the arrows in the magnified views indicate that SCRE was located in the intermediate region of SYCP1-C in the zygotene (O) and pachytene (S) stages. (**T**) Co-localization of SCRE with SYCP1-N, as indicated by the arrow in the magnified view (**U**). (**V**) Co-localization of SCRE with TEX12, as indicated by the arrow in the magnified view (**W**). (**X**) Co-localization of SCRE with SYCE3, as indicated by the arrow in the magnified view (**Y**).

nm. It is known that, for example, the assembly of SYCE2–TEX12 complexes into higher-order filamentous structures is in the range of ∼300–1000 nm. Here, we assumed that the distance between SCRE foci might be related to SYCE2-TEX12 higher order assemblies (21).

Validation of SCRE localization with *Scre*-HA mice

We used the CRISPR/Cas9-mediated genome-editing system to generate a mouse model containing the *Scre* gene with an N-terminal HA epitope tag (23,29). We carried out a detailed analysis of mouse spermatocyte spreads through double labeling with specific antibodies against HA and SYCP3. Consistent with the localization in live testes described above, confocal imaging showed that HA-SCRE was localized as distinct foci along the chromosome axis from the zygotene to the early diplotene stage (Figure 2A–D, arrows). On the XY bivalent, the PAR was also labeled positively for HA-SCRE (Figure 2B, arrow). In the early diplotene stage, SCRE foci disappeared at the desynapsed site (Figure 2C, D, arrowheads), and were not detected in late diplotene stage (Figure 2E). Moreover, SIM imaging showed that HA-SCRE localized specifically to the middle region of developing SCs (Figure 2G, I, arrows). Taken together, these results further verified that SCRE is localized as distinct foci along the CEs of the SC.

Mice lacking *Scre* are infertile

To investigate the functions of SCRE, we generated a gene-deficient *Scre* mouse line using the CRISPR/Cas9 genome editing system (Figure 3A). The *Scre* gene is composed of six exons, with an ATG start codon at the 19th bp of the 94 bp exon 2 and a TGA stop codon in exon 6. The deleted DNA fragment in our knockout mouse model contains exon 3 to exon 6, leaving a remaining 75 bp fragment from ATG in exon 2, which might lead to the translation of a theoretical 25 amino acid peptide. We chose to delete a 5 kb genomic DNA fragment containing exon 3 to exon 6 so that almost all of the coding region was deleted in order to avoid any unpredictable endogenous mRNA splicing alterations or functional compensation of *Scre*. The knockout efficiency was validated by RT-PCR (Supplementary Figure S2A, B).

Neither male nor female mice lacking *Scre* displayed any obvious abnormalities other than being completely sterile. In accordance with this, the male $Scre^{-/-}$ mice exhibited much smaller testes that were about half the size of those from wild-type mice at the age of postnatal day 35 (PD35), and the female $Scre^{-/-}$ mice suffered from underdeveloped ovaries almost without oocytes at the age of PD6 (Figure 3B, C). The epididymides of $Scre^{-/-}$ mice showed a complete absence of sperm (Figure 3G).

Histological analysis of adult $Scre^{-/-}$ testes at PD35 showed that their seminiferous tubules lacked post-meiotic cell types (Figure 3E), while the presence of spermatogonia and Sertoli and Leydig cells was not altered. At PD15, extensive cell death and apoptosis was detected in the seminiferous tubules (Supplementary Figure S3L, arrows), suggesting that *Scre* deficiency already affects spermatocytes during the first wave of meiosis. Histological analysis of whole ovaries of $Scre^{-/-}$ female mice at 6 weeks of age showed the almost complete absence of ovaries (Supplementary Figure S3G, H). We analyzed oocytes from embryonic day E17.5 to PD6 females (Figure 3H–K, Supplementary Figure S3A–F) and found that although $Scre^{-/-}$ ovaries contained abundant numbers of oocytes at E17.5 (Figure 3I), the ovaries were almost entirely devoid of oocytes by PD1, and they completely lacked oocytes by PD6 (Figure 3K). Thus, *Scre* is essential for meiosis in both male and female germ cells and is indispensable for supporting male and female fertility in mice.

SCRE is indispensable for maintaining the integrity of synapsed homologous chromosomes

To identify the intra-nucleus defects in meiotic $Scre^{-/-}$ germ cells, we observed the process of chromosomal synapsis by assessing the distribution of the CE components (i.e. SYCP1-N) and axial/lateral elements (i.e. SYCP3) of the SCs. Spermatocytes at different meiotic stages were quantified from PD35 $Scre^{+/+}$ and $Scre^{-/-}$ testes (Supplementary Figure S4G). Wild-type pachytene spermatocytes contained fully synapsed autosomes and even metaphase I spermatocytes at PD35 (Supplementary Figure S4A–C), whereas the most advanced spermatocytes in the $Scre^{-/-}$ males were only at a pachytene-like stage (Supplementary Figure S4D–F). It is apparent that meiosis prophase I was arrested at the pachytene stage in $Scre^{-/-}$ males.

SIM of SC staining showed that in $Scre^{+/+}$ spermatocytes the SYCP1-N signal was continuous in the synapsed part from the zygotene to diplotene stage (Figure 4A–C; Supplementary Figure S4H). In mutant spermatocytes, however, although the initial SYCP1 assembly (as indicated by the correct SYCP1-N localization) at the early zygotene stage appeared to occur normally in the absence of SCRE (Figure 4D, G), the SC desynapsed prematurely immediately afterwards, with the SYCP1 C-terminus still remaining on the chromosomal axes indicative of a collapsed SC structure (Figure 4E, H; E', H' arrows; Supplementary Figure S4I). At late pachytene-like stage, the SC was completely desynapsed (Figure 4F, I; F', I' arrows). Nevertheless, the possibility formally exists that the central region components first associate with unpaired chromosome axial elements, which prevents further association of these segments and thus failure of synapsis, as in the case of *hal-2* mutations in *C. elegans* (30).

We observed similar defects in meiotic progression in $Scre^{-/-}$ oocytes. Female germ cells enter meiosis shortly after sex determination during embryogenesis, and we observed oocytes at different meiotic stages from E15.5 to PD1 in $Scre^{+/+}$ and $Scre^{-/-}$ ovaries (Supplementary Figure S5I–L). At E15.5, $Scre^{-/-}$ ovaries had no apparent abnormalities compared with wild-type (Supplementary Figure S5A, E). At E17.5, 90% of the oocytes in $Scre^{+/+}$ ovaries had reached the pachytene stage and all 20 chromosome pairs were fully synapsed (Supplementary Figure S5B). With the progression of oocyte development, the homologous chromosomes remained fully synapsed until PD1 (Supplementary Figure S5C, D). In contrast, at E17.5 the $Scre^{-/-}$ ovaries contained very few normal pachytene-stage oocytes. Instead, most of the oocytes were at a pachytene-

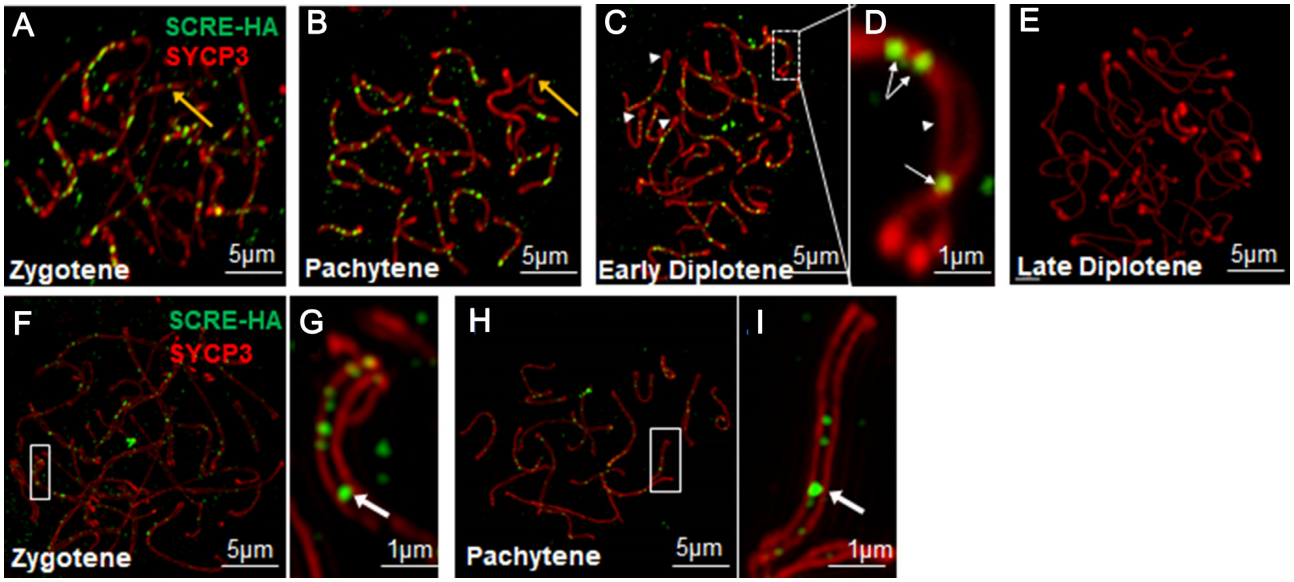

Figure 2. Validation of SCRE localization with HA-*Scre* mice. (**A–E**) SCRE localized on the chromosome axis as distinct foci at the zygotene (**A**), pachytene (**B**), early diplotene (**C**) and late diplotene (**E**) stages. (B, arrow) The PAR of the XY bivalent was labeled positively for SCRE. (**D**) Magnified views of desynapsed regions indicated by arrowheads, synapsed regions colocalized with SCRE indicated by arrows. (**F–I**) SIM images of zygotene (**F**) and pachytene (**H**) nuclei immunolabeled for HA-SCRE and SYCP3, as indicated by the arrows in the magnified views in (**G**) and (**I**).

like stage and were characterized by SC disassembly and unpaired chromosomes still contained the SYCP1-N signal (Supplementary Figure S5F, arrow). As oocyte development progressed, they exhibited more severe desynapsis problems (Supplementary Figure S5G, H arrows). The defects in chromosomal synapsis were similar between *Scre*-deficient spermatocytes and oocytes.

To gain further insight into the synaptic defects, we next double-labeled the spermatocytes with SYCP3 and TEX12 (Figure 4J–U). During early pachytene-like stage, TEX12 assembled with SYCP3 normally in $Scre^{-/-}$ spermatocytes (Figure 4L–P). Subsequently however, TEX12 underwent apparent loss and its expression pattern changed from continuous expression along the chromosome axes into discrete dots (Figure 4Q–U, arrows). SYCE2 also showed similar defects in meiotic progression in $Scre^{-/-}$ spermatocytes (data not shown). These results demonstrate that SCRE is essential for stabilizing chromosomal synapses.

In addition to premature SC desynapsis, in ∼20% of $Scre^{-/-}$ spermatocytes at the first wave of spermatogenesis (before PD35), SCs had formed between several partners (Figure 4V–Y). The earliest irregular synapsis with several partners occurred at the early zygotene stage (Figure 4V, W, arrows), and with the further development of spermatocytes more partners were involved (Figure 4X, Y, arrows). These results indicate that the LE and SC complex formation appears to be normal, but that extended homologous synapsis is impaired in the absence of SCRE in $Scre^{-/-}$ spermatocytes.

$Scre^{-/-}$ spermatocytes exhibited mild defects in DSB repair and impaired crossover formation as a secondary event of instable synapsis

We next examined the process of DSB repair and meiotic recombination. During meiosis, SPO11-generated DSBs lead to phosphorylation of H2AX through the activation of the ATM kinase (31,32). Analysis of chromosome spreads from PD16 to PD35 (i.e. first wave of spermatogenesis) , $Scre^{-/-}$ spermatocytes showed that some phosphorylated H2AX (γH2AX) signal persisted at pachytene-like stage on autosomes that had some AEs synapsed with several partners (Supplementary Figure S4K, arrow). The persistence of γH2AX suggested that some DSBs were not properly repaired (33,34). However, by using chromosome spread prepared from 2 to 6 months adult $Scre^{-/-}$ males, we found that the γH2AX signals have all disappeared in autosomes at the early pachytene-like, mid pachytene-like or late pachytene-like $Scre^{-/-}$ spermatocytes, but the γH2AX signal still existed in XY body (Supplementary Figure S4M–O, blue dotted circles). These γH2AX signals had no apparent difference as compared with $Scre^{+/+}$ spermatocytes in their XY body area (Supplementary Figure S4L, white dotted circles). This result indicated that in adult $Scre^{-/-}$ spermatocytes the DSB repair is not a major event that is affected by the lack of SCRE.

We further explored the distribution of proteins involved in recombination and DSB repair. Interestingly, in the $Scre^{-/-}$ pachytene-like spermatocytes, only the number of RPA2 foci at pachytene-like stage was significantly different (Supplementary Figure S6A), whereas the numbers of RAD51 and DMC1 foci were not significantly different compared with wild type from leptotene to early pachytene stage (Supplementary Figure S6B, C). The increased number of RPA2 foci are consistent with the slower meiosis cell cycle progression observed in $Scre^{-/-}$ spermatocytes (Supplementary Figure S4G). Thus, the $Scre^{-/-}$ cells were largely accumulated at late zygotene stage and at pachytene-like stage, with higher RPA2 signals. These results listed above suggested that in the absence of SCRE, DSB repair

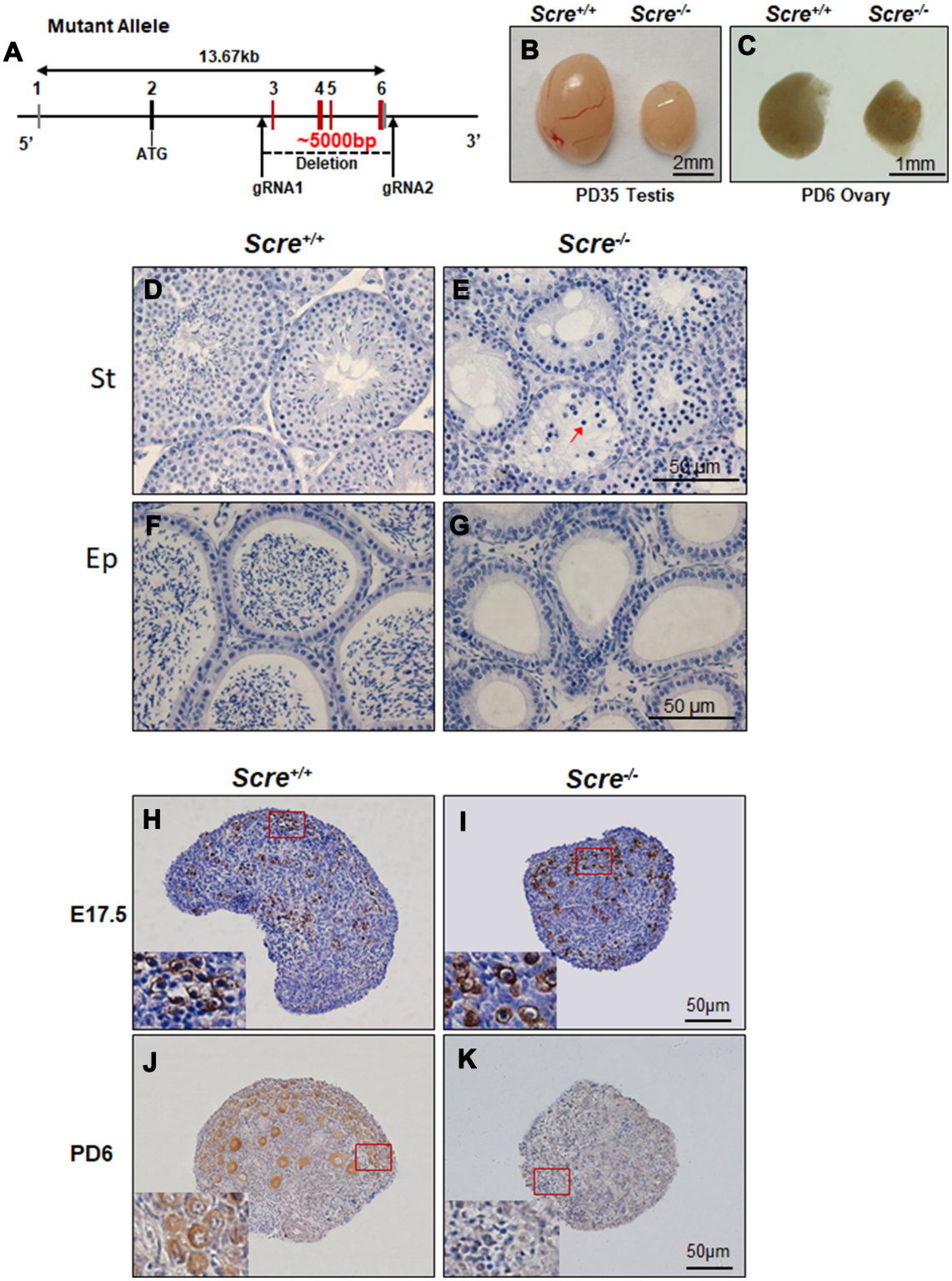

Figure 3. Generation and gonad morphology of $Scre^{-/-}$ mice. (**A**) Schematic representation of the genome editing strategy at the *Scre* locus showing the gRNAs (arrows), the corresponding coding exons (black and red thick lines), and non-coding exons (grey thick lines). Red thick lines (coding exons) represent about 5,000 bp deleted from the wild-type *Scre* allele. ATG, initiation codon. (**B**) $Scre^{-/-}$ male mice had reduced testis size at PD35 ($n = 5$ wild-type and knockout, Welch's *t*-test analysis: $P < 0.0001$). (**C**) $Scre^{-/-}$ female mice had a significant reduction in ovary size at PD6 ($n = 5$ wild-type and knockout, Welch's *t*-test analysis: $P < 0.0001$). (**D**, **E**) $Scre^{-/-}$ male mice had complete arrest of spermatogenesis in epithelial stage IV as shown by hematoxylin-eosin staining of testis sections. Massive apoptosis of spermatocytes is indicated by the arrow. (**F**, **G**) The spermatogenic arrest led to empty epididymides. (St) Seminiferous tubules, (Ep) Epididymides. (**H–K**) Histological analysis of E17.5 and PD6 ovaries from $Scre^{+/+}$ and $Scre^{-/-}$ females. Neonatal ovaries at E17.5 (H, I) and PD6 (J, K) were stained with an anti-DDX4 antibody. $Scre^{-/-}$ ovaries contained abundant numbers of oocytes at E17.5 (I) but were depleted of oocytes by PD6 (K) compared with $Scre^{+/+}$ ovaries.

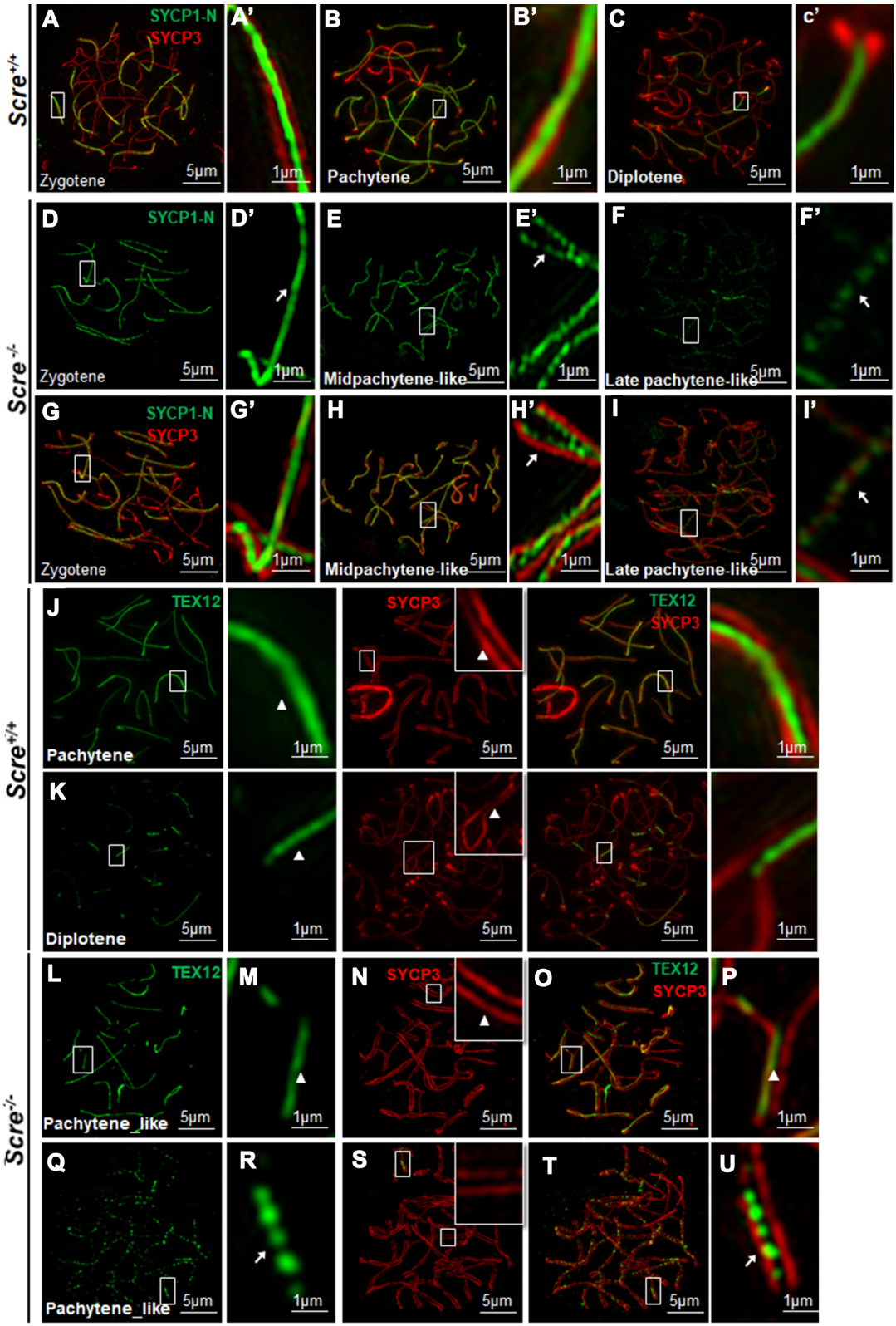
Scre+/+
Scre-/-
Scre+/+
Scre-/-
A
SYCP1-N
SYCP3
Zygotene
5μm
A'
1μm
B
Pachytene
5μm
B'
1μm
C
Diplotene
5μm
c'
1μm
D
SYCP1-N
Zygotene
5μm
D'
1μm
E
Midpachytene-like
5μm
E'
1μm
F
Late pachytene-like
5μm
F'
1μm
G
SYCP1-N
SYCP3
Zygotene
5μm
G'
1μm
H
Midpachytene-like
5μm
H'
1μm
I
Late pachytene-like
5μm
I'
1μm
J
TEX12
Pachytene
5μm
1μm
SYCP3
5μm
TEX12
SYCP3
5μm
1μm
K
Diplotene
5μm
1μm
5μm
5μm
1μm
L
TEX12
Pachytene_like
5μm
M
1μm
N
SYCP3
5μm
O
TEX12
SYCP3
5μm
P
1μm
Q
Pachytene_like
5μm
R
1μm
S
5μm
T
5μm
U
1μm

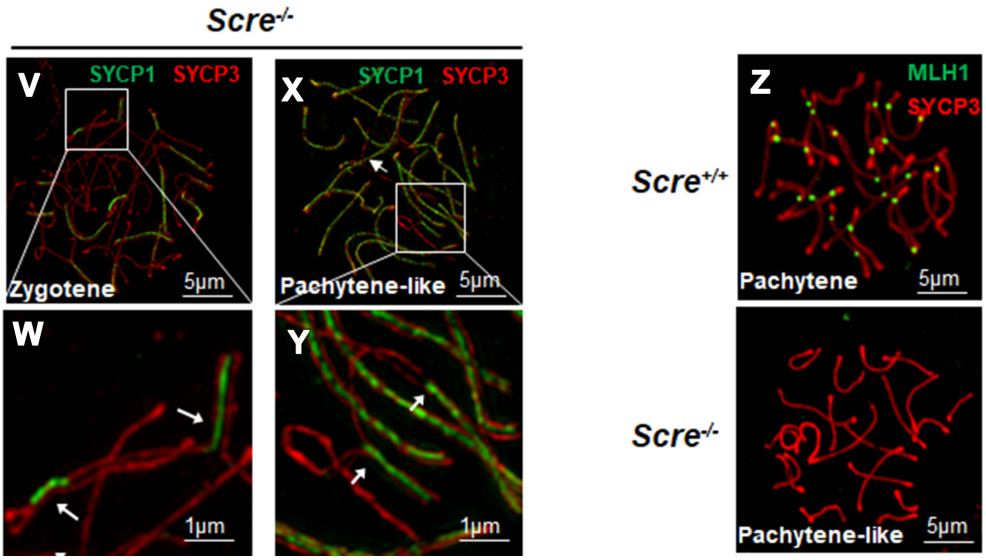

Figure 4. SCRE is essential for stabilizing the SC, and the initiation of synapsis is independent on SCRE. (**A–I**) Spread spermatocyte nuclei immunostained for SYCP3 (red) and SYCP1-N (green) acquired using a super-resolution microscopy. (**A**) Wild-type zygotene nucleus, with the magnified view of the synapsed region (**A'**). (**B**) Wild-type pachytene nucleus, with the magnified view of the synapsed region (**B'**). (**C**) Wild-type diplotene nucleus, with magnified view of the synapsed region (**C'**). (**D, G**) *Scre*$^{-/-}$ spermatocytes at the zygotene stage, with SYCP1 recruited to the chromosome axis. (**E, H**) *Scre*$^{-/-}$ spermatocytes at the mid-pachytene-like stage. (**E', H'**) SCs began to disassemble and the chromosomes began to separate, the 'central localized' SYCP1 N-terminus desynapsed prematurely from each other, as indicated by the arrow. (**F, I**) *Scre*$^{-/-}$ spermatocytes at the late pachytene-like stage showing that SYCP1 localizes in a weak and discontinuous pattern. (**H', I'**) Magnified view showing that SYCP1 localizes at LEs independently of whether LEs are closely aligned or not. (**J–U**) Immunostaining of spread preparations of spermatocytes from the pachytene to diplotene stage with SYCP3 (red) and TEX12 (green) acquired using super-resolution microscopy. (**J, K**) SIM images show that in wild-type spermatocytes from the pachytene to diplotene stage TEX12 localized in a continuous pattern in the synapsed region. (**L, O**) In the early pachytene stage of *Scre*$^{-/-}$ spermatocytes, TEX12 localized in the intermediate region between AEs. (**M, P**) Arrowheads in the magnified views of the synapsed region show that TEX12 localized in a continuous pattern. (**Q, T**) As development progressed, TEX12 localization took the form of discrete foci in the synapsed region as indicated by arrows in the magnified views of the synapsed region (**R, U**). (**V, W**) In the mid-zygotene stage, although only a few bivalent chromosomes that began to synapse were visible, some LEs were synapsed with several partners (arrows). (**X, Y**) Magnified view of a chromosome pair showing that more extensive synapsis occurred in this nucleus, but some LEs were synapsed with several partners (arrows). (**Z**) *Scre*$^{+/+}$ and *Scre*$^{-/-}$ spermatocytes stained for SYCP3 (red) and MLH1 (green).

and meiotic recombination were not the major events that were affected.

MLH1 foci became apparent at the mid-late pachytene stage in *Scre*$^{+/+}$ spermatocytes, marking sites of crossover; but *Scre*$^{-/-}$ spermatocytes did not progress to the mid-late pachytene stage and thus were devoid of MLH1 foci (Figure 4Z). The meiotic defects in fetal oocytes were similar to those observed in spermatocytes from *Scre*$^{-/-}$ mice. All *Scre*$^{-/-}$ pachytene-like oocytes (n = 172) lacked MLH1 foci (Supplementary Figure S6D, E).

SCRE interacts with SYCP1 and SYCE3

To identify the molecular mechanism behind the functions of SCRE in fastening the SC, we co-transfected *GFP-Scre* with cDNAs encoding each of the known CE proteins (*Flag-Syce1, Flag-Syce2, His-Syce3*), cDNAs encoding the transverse filament (TF) protein *Myc-Sycp1* and the LE protein *His-Sycp3*. Our results showed that GFP-SCRE was able to bind Myc-SYCP1 and His-SYCE3, but it was unable to pull down His-SYCP3, Flag-SYCE1 or Flag-SYCE2, implying that SCRE interacted with SYCP1 and SYCE3, but did not interact with SYCP3, SYCE1 or SYCE2 (Figure 5A-E). We then co-transfected with *GFP-Scre, Myc-Sycp1* and *His-Syce3*, and showed that SCRE is able to pull down SYCP1 and SYCE3 at the same time, implying that SCRE might connect SYCP1 and SYCE3 simultaneously and thereby acted as a fastener in the progression of SC formation (Figure 5F).

So far, all SC proteins studied have been proved to exist as homo- or hetero-oligomers (20–22). To determine the possibility of self-association of SCRE, we co-transfected *GFP-Scre* and *His-Scre* and found that GFP-SCRE is able to immunoprecipitate His-SCRE (Figure 5G), suggesting that SCRE might exist as a homo-oligomer.

Based on our results in this paper, we have illustrated our understanding of the interactions among SCRE, SYCP1, and SYCE3 in a model (Figure 6B). In this model, we propose that SCRE acts as a fastener between the transverse filaments and the CE proteins.

DISCUSSION

Synapsis between homologous chromosomes is essential for the completion of meiosis prophase I in mammals, and the SC provides a structural framework for synapsis and for the processing of recombination intermediates into crossovers (1,35). In this work, we have characterized a novel SC protein SCRE. Cytological analysis showed that SCRE colocalizes with CEs and can be precipitated with SYCP1 and SYCE3, indicating that SCRE is a novel component of the CEs and that it plays an essential role in stabilization of the SC in mice. In support of this notion, loss of *Scre* results in premature SC disassembly at late zygotene of spermatocytes

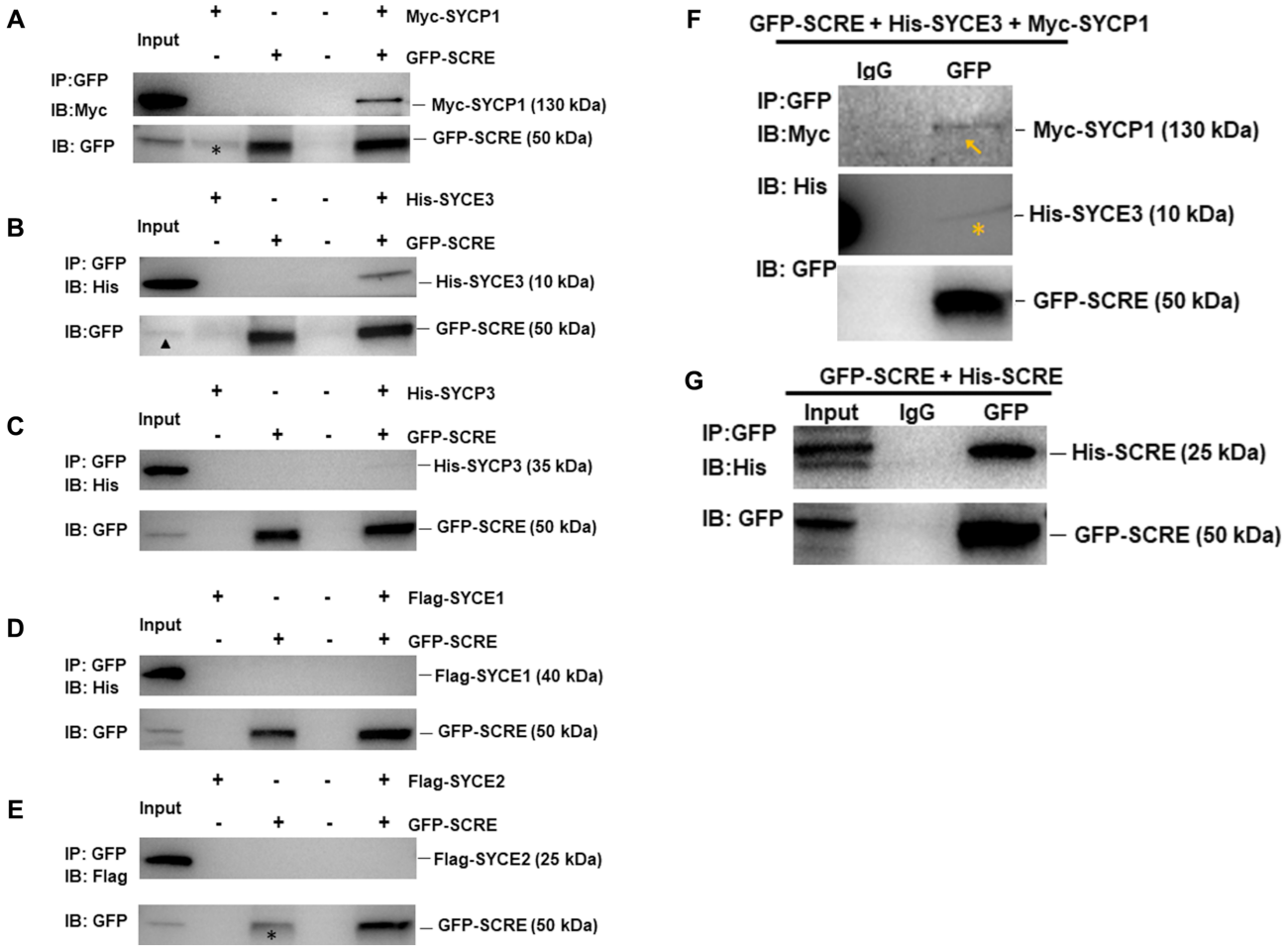

Figure 5. SCRE interacted with SYCP1 and SYCE3 simultaneously (**A–E**) HEK 293T cells were co-transfected with the indicated expression vectors. Protein complexes were immunoprecipitated overnight with anti-GFP antibody and were analyzed by immunoblotting with the indicated antibodies (black asterisks indicate the heavy chain). (**A**) SCRE immunoprecipitated with SYCP1. (**B**) SCRE immunoprecipitated with SYCE3. (**C–E**) SCRE did not interact with SYCP3 (**C**), SYCE1 (**D**), or SYCE2 (**E**). (**F**) HEK 293T cells co-transfected with SCRE, SYCP1, and SYCE3 show that SCRE interacted with SYCP1 (arrow) and SYCE3 (yellow asterisk). (**G**) GFP-SCRE immunoprecipitated with His-SCRE, suggesting that it is able to form at least dimers.

and oocytes. However, a major difference that we observed between SCRE and the other CE components, including SYCP1, SYCE1, SYCE2, SYCE3, TEX12 and SIX6OS1, is that SCRE specifically localizes to the CEs of the SC with a sparse dotted pattern at the synapsed axes of homologous meiotic chromosomes, which is in sharp contrast to the continuous expression pattern of SYCP1, SYCE1, SYCE2, SYCE3, TEX12, and SIX6OS1 seen by immunofluorescence. (16,18,20,36)

We propose that SCRE acts as a fastener reinforcing the linkage between SYCP1-N and SYCE3. The CE contains two discernible subdomains. One domain consists of SYCP1, SYCE3, and SYCE1, of which SYCP1 specifically interacts with SYCE3 and SYCE3 interacts with SYCE1 (37,38). The other domain contains a SYCE2 tetramer and two TEX12 dimers, constituting an equimolar hetero-octamer (21). It has been shown that SYCP1-deficient spermatocytes form normal AEs, which align homologously but do not synapse (16). *Syce1* and *Syce3*-deficient spermatocytes show an intermediate phenotype, with defective recruitment of CE proteins and a weak and discontinuous distribution pattern of SYCP1 along AEs, irrespective of whether they are closely aligned or not (19,39). In this work, although $Scre^{-/-}$ spermatocytes exhibited a similar SYCP1 expression pattern, there was, surprisingly, normal recruitment of CE proteins. However, the CE composition suffered from premature disassembly, or failure of full assembly, at the time when most of the homologous chromosomes had synapsed, leading to arrest at meiosis prophase I and subsequent death of the germ cells. This phenomenon is significantly different from what is seen in spermatocytes that are deficient in other CEs, which arrest at the initiation of chromosome synapsis. Moreover, in $Scre^{-/-}$ spermatocytes, some AEs formed SCs with several partners, showing that the extension of SC proceeded in an incorrect manner. Thus, in the absence of *Scre* the initiation of chromosome synapsis does not seem to be defective, but the accurate elongation and stabilization of the SC is negatively affected. Thus we propose that SCRE is necessary for the proper assembly of CEs.

As for the role of SCRE in DSB repair, we can only see some remaining γH2AX signals on autosomes that

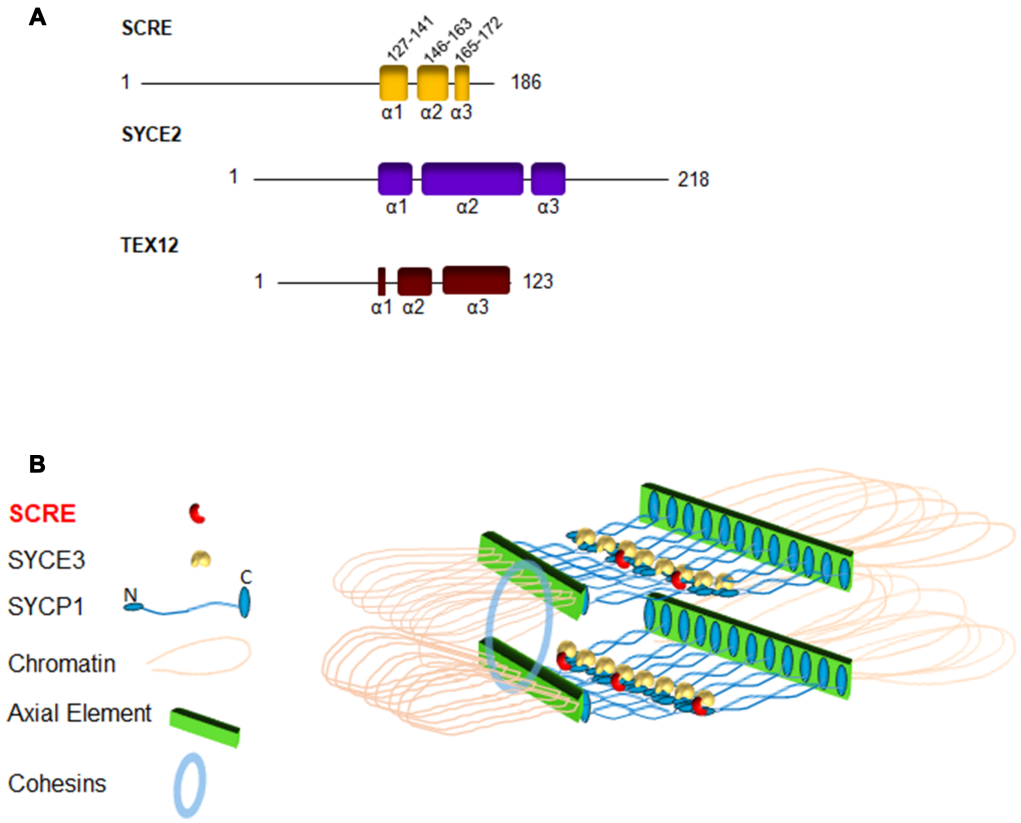

Figure 6. (**A**) Schematic of SCRE, SYCE2 and TEX12 protein sequences. SCRE is consist of 186 amino acids; a-helical structure is predicted for residues 127–141 (α1),146-163 (α2) and 165–172 (α3). SYCE2 is consist of 218 amino acids; a-helical structure is predicted for residues 66–83 (α1), 87–140 (α2) and 143–160 (α3). TEX12 contains 123 amino acids a-helical structure is predicted for residues 52–56 (α1), 62–79 (α2) and 86–121 (α3). Illustrations of the structures of SCRE, SYCE2, and TEX12. For SYCE2 and TEX12, the illustration is adopted and modified from (Davies *et al.*, 2012). (**B**) Homodimers of SYCP1 form unstable N-terminal self-associations and form C-terminal associations with AE components. These associations are stabilized preliminarily by interactions with SYCE3 in the rudiments of the CE. The C-terminus of the SYCP1 molecule is associated with the AE. Then, after interactions are established between SYCP1, SYCE3, SYCE1 and SYCE2, short regions of synapsis begin to extend into completed SCs. Here, SCRE forms discrete foci located at the central region of the SC. The precise quantity and distribution of SCRE in the central region are not clear. SCRE interacts with SYCP1 and SYCE3 simultaneously to stabilize the SC, and SCRE is essential for the stabilization of the SC starting at the early pachytene stage. The structure schematic is only a rough illustration and does not represent the exact structure and localization of the cohesin complex.

had synapsis with multiple partners in the postnatal wave of spermatogenesis. In spermatocytes from adult *Scre*$^{-/-}$ mice, DSBs were completely repaired. These results are consistent with results that foci numbers of RPA2, RAD51 and DMC1 showed no major difference between *Scre*$^{-/-}$ and *Scre*$^{+/+}$ spermatocytes from leptotene to late zygotene stage. Thus, we proposed that SCRE did not directly participate in DSB repair, recombination, and crossover formation. We believe that the complete loss of MLH1-marked chiasmata in *Scre*$^{-/-}$ meiocytes is a consequence of the failure of synapsis caused by the lack of SCRE. In other words, a well fastened SC by SCRE is of great importance for the process of forming and maintaining stable SC, the latter provides the platform for upcoming crossover formation.

In summary, our study identified SCRE as a novel SC protein that is distinct from other known SC proteins. We propose that SCRE serves as a unique SC fastener through reinforcing the integrity of the CE, thereby stabilizing the SC and ensuring meiotic cell cycle progression. We conclude that SCRE is indispensable for the progression of meiosis prophase I in mice.

SUPPLEMENTARY DATA

Supplementary Data are available at NAR Online.

ACKNOWLEDGEMENTS

Author Contributions: K.L., H.L. and Z.C. conceived and designed the entire project. K.L. and H.L. designed and supervised the research. T.H., M.J.L. performed most of the experiments. M.L., Y.Y. and X.Y. performed the co-immunoprecipitation and data analysis. C.Z isolated different stages of male germ cells. J.J., F.Z. and J.L. generated the *Scre*-N-HA mice. K.L., M.J.L. and H.L. wrote the manuscript with contributions from all authors. All authors discussed the results and commented on the manuscript.

FUNDING

National Key Research and Development Programs of China [2017YFC1001100, 2016YFC1000600]; National Natural Science Foundation of China [81771538]; Young Scholars Program of Shandong University [2016WLJH50]; Natural Science Foundation of Shandong Province

[ZR2017MH049]; The *Scre*-N-HA mouse was supplied by the Genome Tagging Project (GTP) Center, SIBCB, CAS, which was supported by Shanghai Municipal Commission for Science and Technology Grants [17411954900]. Funding for open access charge: Shandong University .
Conflict of interest statement. None declared.

REFERENCES

1. Handel,M. and Schimenti,J. (2010) Genetics of mammalian meiosis: regulation, dynamics and impact on fertility. *Nat. Rev. Genet.*, **11**, 124–136.
2. Szekvolgyi,L. and Nicolas,A. (2010) From meiosis to postmeiotic events: homologous recombination is obligatory but flexible. *FEBS J.*, **277**, 571–589.
3. Zickler,D. and Kleckner,N. (2016) A few of our favorite things: Pairing, the bouquet, crossover interference and evolution of meiosis. *Semin. Cell Dev. Biol.*, **54**, 135–148.
4. Agmon,N., Yovel,M., Harari,Y., Liefshitz,B. and Kupiec,M. (2011) The role of Holliday junction resolvases in the repair of spontaneous and induced DNA damage. *Nucleic Acids Res.*, **39**, 7009–7019.
5. Kotwaliwale,C. (2012) Robustness in crossover regulation during meiosis. *Nat. Cell Biol.*, **14**, 335–337.
6. Keeney,S., Giroux,C. and Kleckner,N. (1997) Meiosis-specific DNA double-strand breaks are catalyzed by Spo11, a member of a widely conserved protein family. *Cell*, **88**, 375–384.
7. Baudat,F., Imai,Y. and de Massy,B. (2013) Meiotic recombination in mammals: localization and regulation. *Nat. Rev. Genet.*, **14**, 794–806.
8. Keeney,S. and Neale,M. (2006) Initiation of meiotic recombination by formation of DNA double-strand breaks: mechanism and regulation. *Biochem. Soc. Trans.*, **34**, 523–525.
9. Wold,M. (1997) Replication protein A: a heterotrimeric, single-stranded DNA-binding protein required for eukaryotic DNA metabolism. *Annu. Rev. Biochem.*, **66**, 61–92.
10. Byrne,B. and Oakley,G.G. (2018) Replication protein A, the laxative that keeps DNA regular: The importance of RPA phosphorylation in maintaining genome stability. *Semin. Cell Dev. Biol.*, **86**, 112–120.
11. Tarsounas,M., Morita,T., Pearlman,R. and Moens,P. (1999) RAD51 and DMC1 form mixed complexes associated with mouse meiotic chromosome cores and synaptonemal complexes. *J. Cell Biol.*, **147**, 207–220.
12. Woglar,A. and Villeneuve,A. (2018) Dynamic architecture of DNA repair complexes and the synaptonemal complex at sites of meiotic recombination. *Cell*, **173**, 1678–1691.
13. Allers,T. and Lichten,M. (2001) Differential timing and control of noncrossover and crossover recombination during meiosis. *Cell*, **106**, 47–57.
14. Lynn,A., Soucek,R. and Borner,G. (2007) ZMM proteins during meiosis: crossover artists at work. *Chromosome Res.*, **15**, 591–605.
15. Kolas,N., Yuan,L., Hoog,C., Heng,H.H., Marcon,E. and Moens,P.B. (2004) Male mouse meiotic chromosome cores deficient in structural proteins SYCP3 and SYCP2 align by homology but fail to synapse and have possible impaired specificity of chromatin loop attachment. *Cytogenet. Genome Res.*, **105**, 182–188.
16. de Vries,F., de Boer,E., van den Bosch,M., Baarends,W.M., Ooms,M., Yuan,L., Liu,J.G., van Zeeland,A.A., Heyting,C. and Pastink,A. (2005) Mouse Sycp1 functions in synaptonemal complex assembly, meiotic recombination, and XY body formation. *Genes Dev.*, **19**, 1376–1389.
17. Hamer,G., Gell,K., Kouznetsova,A., Novak,I., Benavente,R. and Höög,C. (2006) Characterization of a novel meiosis-specific protein within the central element of the synaptonemal complex. *J. Cell Sci.*, **119**, 4025–4032.
18. Bolcun-Filas,E., Costa,Y., Speed,R., Taggart,M., Benavente,R., De Rooij,D.G. and Cooke,H.J. (2007) SYCE2 is required for synaptonemal complex assembly, double strand break repair, and homologous recombination. *J. Cell Biol.*, **176**, 741–747.
19. Bolcun-Filas,E., Speed,R., Taggart,M., Grey,C., de Massy,B., Benavente,R. and Cooke,H.J. (2009) Mutation of the mouse Syce1 gene disrupts synapsis and suggests a link between synaptonemal complex structural components and DNA repair. *PLoS Genet.*, **5**, e1000393.
20. Gomez,H., Natalia,F.-M., Manuel,S.-M., Owen,R.D., Isabel,R., Ignacio,G.-T., Dirk,G.R., Ihsan,D., Attila,T., José Luis,B. *et al.* (2016) C14ORF39/SIX6OS1 is a constituent of the synaptonemal complex and is essential for mouse fertility. *Nat. Commun.*, **7**, 13298.
21. Davies,O., Maman,J. and Pellegrini,L. (2012) Structural analysis of the human SYCE2-TEX12 complex provides molecular insights into synaptonemal complex assembly. *Open Biol.*, **2**, 120099.
22. Dunce,J., Dunne,O.M., Ratcliff,M., Millán,C., Madgwick,S., Usón,I. and Davies,O.R. (2018) Structural basis of meiotic chromosome synapsis through SYCP1 self-assembly. *Nat. Struct. Mol. Biol.*, **25**, 557–569.
23. Zhong,C., Yin,Q., Xie,Z., Bai,M., Dong,R., Tang,W., Xing,Y.H., Zhang,H., Yang,S., Chen,L.L. *et al.* (2015) CRISPR-Cas9-Mediated Genetic Screening in Mice with Haploid Embryonic Stem Cells Carrying a Guide RNA Library. *Cell Stem Cell*, **17**, 221–232.
24. Gan,H., Wen,L., Liao,S., Lin,X., Ma,T., Liu,J., Song,C.X., Wang,M., He,C., Han,C. *et al.* (2013) Dynamics of 5-hydroxymethylcytosine during mouse spermatogenesis. *Nat. Commun.*, **4**, 1995.
25. Shibuya,H., Morimoto,A. and Watanabe,Y. (2014) The dissection of meiotic chromosome movement in mice using an in vivo electroporation technique. *PLoS Genet.*, **10**, e1004821.
26. Peters,A., Plug,A., van Vugt,M. and de Boer,P. (1997) A drying-down technique for the spreading of mammalian meiocytes from the male and female germline. *Chromosome Res.*, **5**, 66–68.
27. Schucker,K., Holm,T., Franke,C., Sauer,M. and Benavente,R. (2015) Elucidation of synaptonemal complex organization by super-resolution imaging with isotropic resolution. *Proc. Natl. Acad. Sci. U.S.A.*, **112**, 2029–2033.
28. Kaniecki,K., De Tullio,L. and Greene,E. (2018) A change of view: homologous recombination at single-molecule resolution. *Nat. Rev. Genet.*, **19**, 191–207.
29. Li,Q., Li,Y., Yang,S., Huang,S., Yan,M., Ding,Y., Tang,W., Lou,X., Yin,Q., Sun,Z., Lu,L. *et al.* (2018) CRISPR-Cas9-mediated base-editing screening in mice identifies DND1 amino acids that are critical for primordial germ cell development. *Nat. Cell Biol.*, **20**, 1315–1325.
30. Zhang,W., Miley,N., Zastrow,M.S., MacQueen,A.J., Sato,A., Nabeshima,K., Martinez-Perez,E., Mlynarczyk-Evans,S., Carlton,P.M., Villeneuve,A.M. *et al.* (2012) HAL-2 promotes homologous pairing during Caenorhabditis elegans meiosis by antagonizing inhibitory effects of synaptonemal complex precursors. *PLoS Genet.*, **8**, e1002880.
31. Fernandez-Capetillo,O., Liebe,B., Scherthan,H. and Nussenzweig,A. (2003) H2AX regulates meiotic telomere clustering. *J. Cell Biol.*, **163**, 15–20.
32. Bellani,M., Romanienko,P., Cairatti,D. and Camerini-Otero,R. (2005) SPO11 is required for sex-body formation, and Spo11 heterozygosity rescues the prophase arrest of Atm-/- spermatocytes. *J. Cell Sci.*, **118**, 3233–3245.
33. Rogakou,E., Pilch,D., Orr,A., Ivanova,V. and Bonner,W. (1998) DNA double-stranded breaks induce histone H2AX phosphorylation on serine 139. *J. Biol. Chem.*, **273**, 5858–5868.
34. Jasin,M. and Rothstein,R. (2013) Repair of strand breaks by homologous recombination. *Cold Spring Harb. Perspect. Biol.*, **5**, a012740.
35. Henderson,K. and Keeney,S. (2005) Synaptonemal complex formation: where does it start? *Bioessays*, **27**, 995–998.
36. Lu,J., Gu,Y., Feng,J., Zhou,W., Yang,X. and Shen,Y. (2014) Structural insight into the central element assembly of the synaptonemal complex. *Sci. Rep.*, **4**, 7059.
37. Hernandez-Hernandez,A., Masich,S., Fukuda,T., Kouznetsova,A., Sandin,S., Daneholt,B. and Höög,C. (2016) The central element of the synaptonemal complex in mice is organized as a bilayered junction structure. *J. Cell Sci.*, **129**, 2239–2249.
38. Fraune,J., Schramm,S., Alsheimer,M. and Benavente,R. (2012) The mammalian synaptonemal complex: protein components, assembly and role in meiotic recombination. *Exp. Cell Res.*, **318**, 1340–1346.
39. Schramm,S., Fraune,J., Naumann,R., Hernandez-Hernandez,A., Höög,C., Cooke,H.J., Alsheimer,M. and Benavente,R. (2011) A novel mouse synaptonemal complex protein is essential for loading of central element proteins, recombination, and fertility. *PLoS Genet.*, **7**, e1002088.